

# Doing More with Less: A Method for Low Total Mass, Affinity Measurement Using Variable-Length Nanotethers

Richard D. Perrins,<sup>†</sup> Craig Orchard,<sup>†</sup> Maria Zavodszky,<sup>‡</sup> Amal Kasry,<sup>†,§</sup> Nikolay Nikolaev,<sup>†,||</sup> Adrian Harwood,<sup>†</sup> Paola Borri,<sup>†</sup> and Trevor Dale<sup>\*,†</sup>

<sup>†</sup>Cardiff School of Biosciences, Biomedical Sciences Building, Museum Avenue, Cardiff, CF10 3AX, U.K.

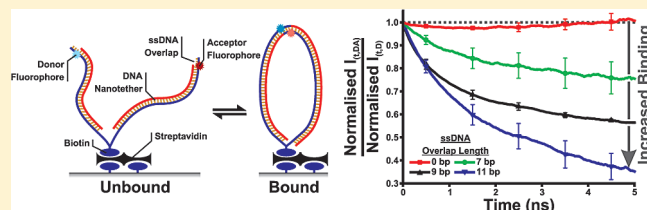
<sup>‡</sup>GE Global Research, 1 Research Circle, Niskayuna, New York 12309, United States

<sup>§</sup>IBM T. J. Watson Research Center, 1101 Kitchawan Road, Yorktown Heights, New York 10598, United States, and Egypt Nanotechnology Center (EGNC), Smart Village, Giza 12577, Egypt

<sup>||</sup>Wolfson School of Mechanical & Manufacturing Engineering, Loughborough University, Loughborough LE11 3TU, U.K.

**S** Supporting Information

**ABSTRACT:** Interactions between biomolecules are an important feature of biological systems and understanding these interactions is a key goal in biochemical studies. Using conventional techniques, such as surface plasmon resonance and isothermal titration calorimetry, the determination of the binding constants requires a significant amount of time and resources to produce and purify sufficient quantities of biomolecules in order to measure the affinity of biological interactions. Using DNA hybridization, we have demonstrated a new technique based on the use of nanotethers and time-resolved Forster resonance energy transfer (FRET) that significantly reduces the amount of material required to carry out quantitative binding assays. Test biomolecules were colocalized and attached to a surface using DNA tethers constructed from overlapping oligonucleotides. The length of the tethers defines the concentration of the tethered biomolecule. Effective end concentrations ranging from 56 nM to 3.8  $\mu$ M were demonstrated. The use of variable length tethers may have wider applications in the quantitative measurement of affinity binding parameters.



Interactions between biomolecules are crucial to function and the determination of their affinity is a key goal in the analysis of biological systems. Quantitative biochemical affinity measurement techniques, such as surface plasmon resonance<sup>1</sup> and isothermal titration calorimetry,<sup>2</sup> require significant masses of purified biomolecules to saturate binding. Fluorescence-based techniques have been shown to work with low total masses when studying high affinity interactions such as antibody–antigen interactions.<sup>3</sup> However, many important interactions such as those involved in the formation of multiprotein complexes are medium to low affinity and require high concentrations of purified proteins in the solution phase to measure biological affinities. The mass and purity requirements inherent to these techniques slow research progress due to the outlay of resources and time required for biomolecule production.

By contrast, numerous techniques have been developed that detect low concentrations of biomolecules in high throughput array formats. Here, the measurement of affinity is less important than the quantification of abundance combined with high specificity.<sup>4</sup> In general, array techniques work best with high affinity interactions and when the biomolecule concentration is many times higher than the dissociation constant. Array technologies are particularly common in nucleic acid analysis where the intrinsic specificity and high affinity of hybridization can be exploited for efficient nucleic acid quantification.

However, a technique that is able to provide accurate quantitative measurements of binding affinities in an array format without requiring large masses of purified biomolecules is still missing. Here we demonstrate that variable-length DNA tethers can be used in a predictable way to measure the affinity of intermolecular interactions in a novel technique termed “nanotether biochemistry”.

The coupling of biomolecules has been used to enhance intermolecular interactions in a range of analytical techniques. For example, intramolecular interactions between calmodulin and a calmodulin-binding subsequence have been coupled to CFP and YFP fluorophores, via a linker/tether sequence, allowing Forster resonance energy transfer (FRET) between the fluorophores to be used in Ca<sup>2+</sup> sensing.<sup>5</sup> Assays that read out the formation or breaking of intramolecular interactions have also been developed for protein kinase and protease activities as detected by changes in FRET that requires a close molecular proximity (<10 nm).<sup>6</sup> Similar in concept are sensitive nucleic acid detection technologies that rely on a reduction of FRET between two fluorophores located at either end of a hairpin

**Received:** May 17, 2011

**Accepted:** October 26, 2011

**Published:** October 26, 2011

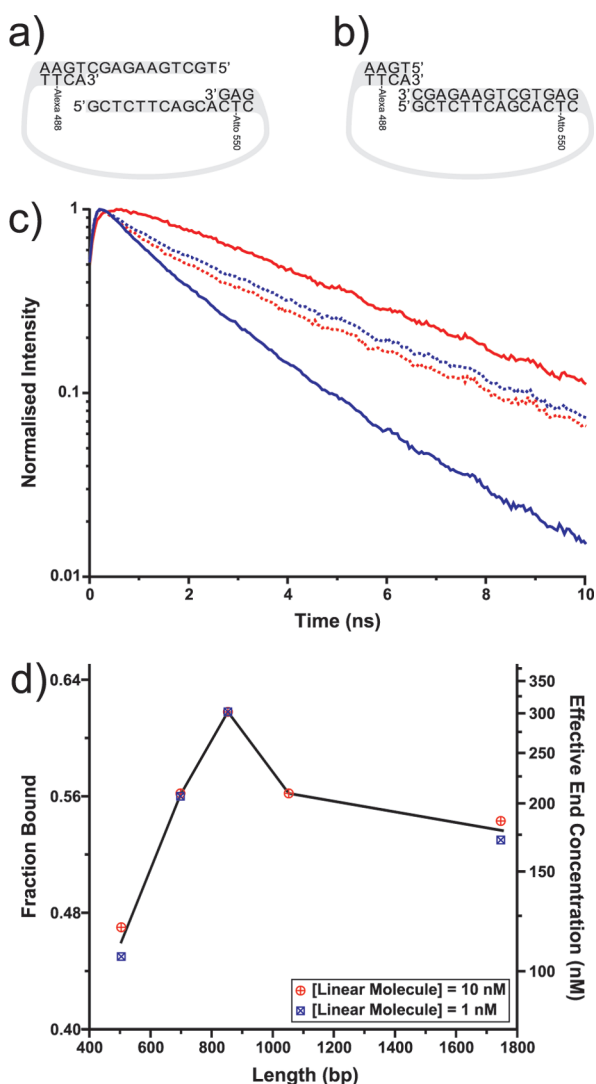


**Figure 1.** Length-dependent but concentration-independent binding of DNA in solution. (a) Schematic of a linear molecule containing an 11 bp overlap and the position of the donor (Alexa Fluor 488) and acceptor fluorophores (Atto 550). (b) Schematic of a linear molecule without complementary ssDNA overlaps, the 0 bp overlap. (c) Fluorescence intensity decay from donor (blue) and acceptor (red) fluorophores for an 504 bp linear molecule with an 11 bp (solid line) or 0 bp (dashed line) overlap. The hybridization-dependent decrease in donor lifetime coincides with an increase in the acceptor fluorophore lifetime. (d) The fraction of headset binding was calculated from the change in donor fluorescence lifetime and was related to the effective end concentration based on the 71 nM affinity of the 11 bp overlap that was independently determined. The fraction of binding was measured for the linear DNAs shown.

ssDNA sequence following the unfolding that accompanies hybridization to a target.<sup>7</sup>

In the nanotether system the two interacting biomolecules are attached to a variable length tether. By changing the length of the tether, the effective local concentration of the tethered biomolecules (end concentration) can be altered. The tethers should be made from a material that can be readily synthesized in a range of different lengths and have the ability to self-assemble onto a surface attached anchor. DNA fulfils these criteria and can be chemically synthesized, as a series of overlapping oligonucleotides, with a wide

variety of functional groups to further facilitate its function as part of a nanotether device.

There have been a number of theoretical and experimental studies analyzing length-dependent “DNA looping” in which the interaction of the DNA “free-ends” was measured by the efficiency of end ligation.<sup>8</sup> These studies showed that a key property of linear polymers that determines the frequency of end-to-end encounters (and therefore the equivalent “end concentration”) is the persistence length of the polymer.<sup>9</sup> A higher persistence length is associated with a stiffer polymer. For double stranded DNA, the persistence length has been estimated at 150 bp; this contrasts with a length of 2–6 nucleotides for ssDNA.<sup>8–10</sup> For dsDNA, a relationship between DNA length and end concentration can be established and used to predict the concentration of the free ends.

Using single-stranded DNA overlaps with known affinities as the tethered biomolecule, we have shown length-dependent control of biomolecular association both with DNA in solution and with DNA tethers on a surface. The approach should allow the measurement of both low and high affinity interactions using very low masses of biomolecules and is compatible with high throughput array technologies.

## MATERIALS AND METHODS

**Oligonucleotides.** HPLC purified oligonucleotides were ordered from Biomers.net (see Table S1 in the Supporting Information for sequences). Where indicated, oligonucleotides contained the labeled bases dT-Atto 488 (labeled 6 in the sequences shown in Table S1 in the Supporting Information), dT-Atto 550 (labeled 8), dT-Alexa 488 (labeled 9), and C3 spacers (labeled 7). Oligonucleotides V5NM-11 and 5C488NM were 5′ phosphorylated while the blocking oligonucleotide contained a 5′ biotin modification.

The Y-shaped anchor oligonucleotide (Biomers.net) effectively consists of two oligonucleotides. The sequence of the first oligo is 5′-ACTGGGTGACTTCAGACGGTTTT(dT-Biotin)-3′. The second has the sequence 5′-ACGGTTCGAATGACCCGTGGTTT-3′ and is attached, via a 3′ phosphate, to the 3′ end of the first oligonucleotide (Figure 2a).

**Arm Assembly.** Nanotether arms were assembled by heating and then slowly cooling equimolar concentrations of the indicated oligonucleotides. In total, 0.2 μM of each HPLC-purified oligonucleotide required to synthesize the nanotether arm (see Figure S1 and Table S2 in the Supporting Information) was mixed with 0.2 μM of the appropriate headset oligonucleotide (H1ds0, H1ds7, H1ds9, H1ds11, H1ns11, H2as11, or H2ns11) in hybridization buffer (10 mM HEPES, pH 7, 150 mM NaCl, 5 mM EDTA), and the solution was heated to 95 °C and then cooled to 4 °C over 11 min.

**Surface Preparation.** Streptavidin-coated coverslips (24 mm × 50 mm, thickness no. 1.5) were prepared as previously outlined.<sup>11</sup> A thin layer of silicone grease was applied to both sides of a 50 × 7 μL chambered coverslip gasket (Grace Bio-Laboratories). The greased gasket was then carefully applied to the treated face of a streptavidin-coated coverslip to generate an array of surfaces for subsequent binding experiments.

Each well was washed once with 10 μL of hybridization buffer (10 mM HEPES, pH 7, 150 mM NaCl, 5 mM EDTA). A 6 μL volume of oligonucleotide anchor solution (50 nM Y-shaped anchor oligo, 150 nM biotinylated “blocking oligonucleotide”, 1 × hybridization buffer) was applied to each well. The blocking

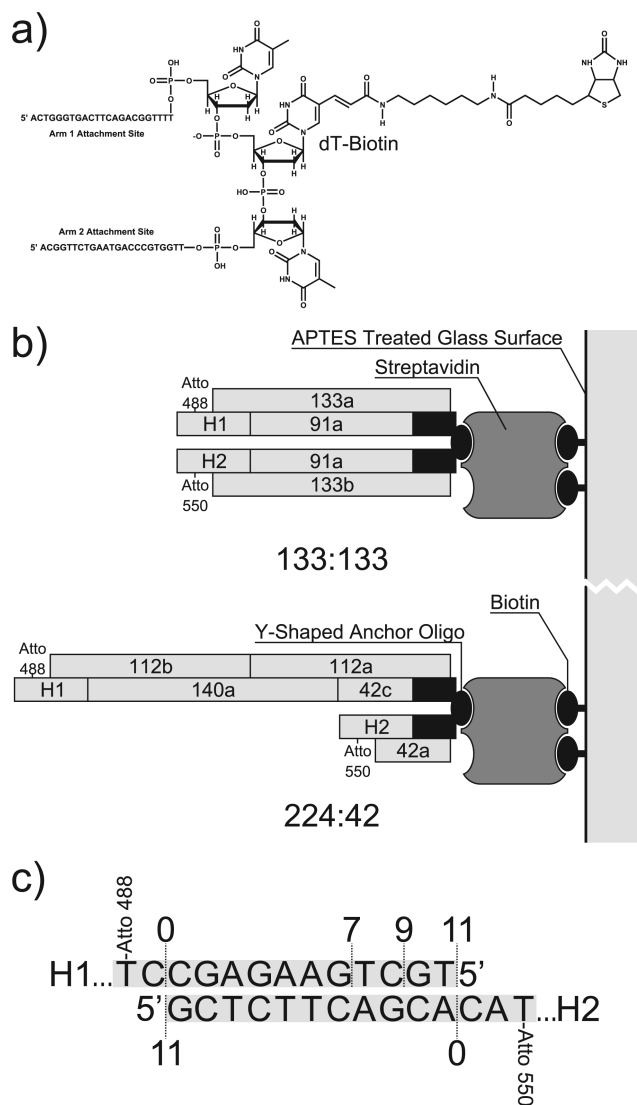


**Figure 2.** Construction of the surface attached Y-shaped nanotethers. (a) The structure of the Y-shaped anchor oligonucleotide. (b) Streptavidin was used to attach the Y-shaped anchor oligo to the biotinylated glass surface.<sup>11</sup> Nanotether arms were constructed from equimolar mixtures of overlapping oligos and were hybridized to the anchor oligo to form the nanotether. Headsets (H1 and H2) consist of an interacting biomolecule attached to an oligonucleotides complementary to the end of nanotether. This is used to attach the biomolecule to the tether. H1 and H2 are labeled with donor (Atto 488) and acceptor (Atto 550) fluorophores. (c) The acceptor fluorophore (Atto 550) labeled headset, H2, had either an 11 or 0 bp overlap, while the donor fluorophore (Atto 488) labeled headset, H1, was staggered in length to generate either an 11, 9, 7, or 0 bp overlap.

oligonucleotide was used to control the density of the Y-shaped anchor attached on the surface (see the Supporting Information for further discussion). The coverslip was then incubated at room temperature, in a sealed humid environment to minimize evaporation, for 30 min. The wells were washed twice with 10  $\mu\text{L}$  of hybridization buffer. Equal volumes of 0.2  $\mu\text{M}$  nanotether arm 1 and arm 2 solutions, containing the desired arm lengths, were mixed and 6  $\mu\text{L}$  of this solution and was applied to the desired wells followed by room temperature hybridization in a sealed humid environment for 30 min. The wells were then washed

twice with hybridization buffer before being filled with 8  $\mu\text{L}$  of hybridization buffer and sealed with a clean 24 mm  $\times$  50 mm (thickness no. 1.5) coverslip placed over the gasket. The samples were measured using time-resolved FRET as described in the Supporting Information.

**Headset Affinity Determination.** A greased 50  $\times$  7  $\mu\text{L}$  chambered coverslip gasket was placed onto an unmodified 24 mm  $\times$  50 mm coverslip (thickness no. 1.5). Two headsets comprising two oligonucleotides each were used in titration experiments. Both donor and acceptor oligonucleotide pair concentrations were varied in parallel from 50 nM to 10  $\mu\text{M}$  as indicated. To generate the 11 bp overlap pair, equimolar amounts of H1ds11 were hybridized with HS-end-comp to make the donor headset H1. The acceptor headset H2 was similarly generated from oligonucleotides H2as11 and HS-end-comp. Shorter overlap head-set pairs were generated by substituting H1ds11 for H1ds9, H1ds7. The 0 bp overlap pair was generated from H1ds0 + HS-end-comp (donor) together with H2as0 + HS-end-comp (acceptor). The chambers were then sealed with a top coverslip and the samples measured using time-resolved FRET. Donor-only and acceptor-only measurements were taken in the absence of the partner headset. The use of unlabeled oligonucleotides in place of one of the labeled headsets gave identical results to that of headset removal (data not shown).

**Linear Molecule Preparation.** Various lengths of the mouse Axin 1 gene were amplified, by PCR, and inserted into the pCR2.1-TOPO plasmid (Invitrogen). Plasmids were digested with BstXI (NEB) yielding three different length inserts with incompatible 4 bp 3' sticky ends. The variable DNAs were purified by agarose gel electrophoresis followed by gel extraction. Donor and acceptor headset oligonucleotides were then ligated to the purified fragments. Donor headset dsDnm-11 was prepared by heating 25  $\mu\text{M}$  5C488NM and 25  $\mu\text{M}$  V3NMM-11 in annealing buffer (70 mM NaCl, 10 mM Tris, pH 8.0) at 95  $^{\circ}\text{C}$  for 2 min then slowly cooling to 4  $^{\circ}\text{C}$  over 90 min. Acceptor headset dsAnm-11 was prepared in a similar manner using 25  $\mu\text{M}$  3C550NM and 25  $\mu\text{M}$  V5NM-11. T4 ligase (NEB) was used to ligate 3  $\mu\text{M}$  annealed headset to 20  $\text{ng } \mu\text{L}^{-1}$  purified fragments. The ligated linear molecules were purified by agarose gel electrophoresis. Samples were measured for time-resolved FRET as for the headset titrations.

**Molecular Simulations.** Monte Carlo simulations were performed using CarChy++.<sup>12</sup> The DNA was modeled as a chain of 50 nm persistence length, composed of charged, rigid, 4 nm long segments connected by flexible joints. Interactions between the segments included hydrodynamic and electrostatic interactions as well as harmonic spring potentials for bending, torsion, and stretching. Y-shaped DNA nanotether arm pairs were represented by an open-ended double stranded DNA with one free joint. The local concentration of the free ends within a sphere having a 10 nm radius around one end was calculated for various total DNA lengths (80–720 nm) and arm length ratios (1:9 to 1:1). Simulations for short tether length were not possible due to the unit chain-length used in the simulation (manuscript in preparation).

## RESULTS AND DISCUSSION

**Length-Dependent and Concentration-Independent Association of ssDNA Overlaps in Solution.** As a test biomolecular interaction, we focused on complementary single stranded DNA overlaps because they generate a uniform molecular

orientation for interactions with distinct affinities specified by the length of their overlap. In the experiments that follow, 0 bp, 7 bp, 9 bp, and 11 bp nonpalindromic interactions were generated from a set of four oligonucleotides to form a pair of “headsets” that were analyzed in free solution, attached to either end of a linear DNA molecule (Figure 1a) or attached, in a modified form, to each of two arms of an immobilized Y-shaped molecule (Figure 2b). Hybridization of the single stranded overlaps was detected by time-resolved FRET between the Atto 488 (Alexa Fluor 488 in the initial linear DNA molecule experiments) and Atto 550 dyes attached as illustrated in Figure 1 (5.4 nm apart based on 0.34 nm/base pair).

When donor and acceptor headsets were attached to either end of a 504 bp linear DNA, a strong decrease in the lifetime of the donor fluorophore and a corresponding increase in the emission of the acceptor fluorophore was observed for the 11 bp but not for the 0 bp DNA overlap (Figure 1c). Studies with an 11 bp overlap set that lacked an acceptor fluorophore (donor-only) showed no FRET suggesting that the rate of donor decay could be used as an accurate measure of the proportion of bound and free biomolecules.

In this experimental format, changes in time-resolved fluorescence have a clear advantage when compared to measuring FRET efficiency by the change in donor and acceptor fluorescence intensities. This is because donor and acceptor lifetimes were measured to be independent of fluorophore concentration and laser excitation intensity (in the range of concentrations and low excitations  $<100 \mu\text{W}/\text{mm}^2$  used in the experiments) and hence are not susceptible to differences in fluorophore concentration between samples or laser excitation instabilities, while absolute intensity measurements are. Bleed-through of the donor or acceptor fluorescence into the adjacent channel is a relative intensity correction and can be easily subtracted using this method.

Titration of free “donor” and “acceptor” 11 bp overlap headsets showed that the affinity of the 11 bp overlap was 71 nM in 150 mM NaCl, 10 mM HEPES, pH 7, 5 mM EDTA (Figure S2a in the Supporting Information). On the basis of an affinity of 71 nM for the 11bp overlap, the 504 bp linear molecule was calculated to generate an effective free end concentration of 110 nM.

Attachment of the 11 bp overlap to 504, 698, 853, 1052, and 1752 bp linear tethers showed that different length tethers generated distinct effective end concentrations with a maximum behavior as predicted from previous theoretical and experimental measurements of interend concentrations using techniques including end ligation<sup>8</sup> and Monte Carlo modeling.<sup>13</sup> Importantly, the fraction of bound linear molecules was not altered by a 10-fold dilution demonstrating that intra- rather than intermolecular interactions were predominantly responsible for the TR-FRET signal (Figure 1d).

**Tether Length-Dependent Binding on a Surface Using a Y-Shaped Molecule.** Because of the intrinsic stiffness of linear DNA, short linear DNA molecules were predicted (and found) to generate maximal end concentrations in the range of 100–300 nM under the experimental conditions used (Figure 1d). To increase the end concentration, we “broke” the linear molecules into two distinct arms that were anchored via a flexible Y-shaped anchor molecule (Figure 2). A biotin molecule was placed at the base of the Y-shaped anchor to allow tether assembly to be carried out on a surface. As previously shown, a glass surface modified with a protocol including a final streptavidin coupling

step proved to be optimal for high density attachment with low nonspecific background and free diffusion of DNA ends.<sup>11</sup> The amount of Y-shaped anchor attached to the surface was controlled by the addition of a biotinylated blocking oligo with the ratio of these two oligos optimized in order to minimize cross-talk between adjacent nanotether pairs (details in the Supporting Information).

Significant fractions of bound donor were observed, via TR-FRET, from 7 bp, 9 bp, and 11 bp overlaps at the free ends of symmetrical 42 bp tethers (Figure 3a). The highest fraction was detected with the 11 bp followed by the 9 bp and then the 7 bp overlap. This was expected since the dissociation constants of the overlaps were determined to be  $>10 \mu\text{M}$  for the 7 bp overlap, 850 nM (SD = 40 nM,  $n = 3$ ) for the 9 bp overlap, and 71 nM (SD = 1.5 nM,  $n = 2$ ) for the 11 bp overlap (Figures S2a–c in the Supporting Information). Further analyses of tether length-dependence particularly focused on the 9 bp overlap since it generated clear TR-FRET while binding was not saturated using the tether lengths under analysis. When symmetrical tethers of 224 bp, 133 bp, 63 bp, and 42 bp were used with the 9 bp overlap, clear length dependence was observed in which shorter tethers generated higher levels of bound molecules (Figure 3b). On the basis of the 850 nM affinity of the 9 bp overlap, the effective end concentration generated by the 42 bp tether was calculated to be  $3.8 \mu\text{M}$ , a concentration much higher than can be generated by linear DNA. Longer tether lengths generated lower effective concentrations as expected by their ability to explore a larger volume (Figure 3c).

Numerical Monte Carlo modeling of effective end concentrations, using a model for linear DNA which was modified to include a totally flexible hinge at the midpoint between the two arms, showed a similar trend to experimental observations although measured end concentrations were lower than calculated (Figure 3c). This could be due to several factors. The simulations did not account for the role of the surface that may restrict the movement of the tether arms. The simulation also lacked any interactions between adjacent arm-pairs, solvent effects, the transmission of Brownian motion from the tether body to the binding interaction, the presence of nicks in the sugar–phosphate backbone, or DNA-sequence specific changes in DNA structure or flexibility.

Modeling further suggested that tether lengths required to generate low nanomolar concentrations of free ends would be more than 1 kilobase in length ( $>300 \text{ nm}$ ) and would therefore have to be sparsely distributed on the chip surface, to avoid interactions between adjacent tethered molecule-pairs, leading to a reduction in signal intensity. To overcome this potential problem, we investigated the use of asymmetric tether arm lengths since modeling further suggested that DNA stiffness could be used to reduce the probability that a long tether would fold back to interact with the free-end of a shorter arm, thereby reducing the effective concentration (Figure 3d). Initial experiments maintained a fixed total tether length of 266 bp (arm 1 length + arm 2 length = total tether length; Figure 3e). The effective end concentrations from the 133:133, 161:105, 182:84 nanotether arm configurations (ratios 1, 0.65, and 0.46, respectively) followed the general trend of effective end concentrations calculated from simulations (Figure 3e). However, the effective end concentrations of one configuration (224:42; ratio 0.19) diverged from the simulation-derived concentrations. This may be due to a number of possible factors including sequence-specific conformations of the nanotether pair or the relative

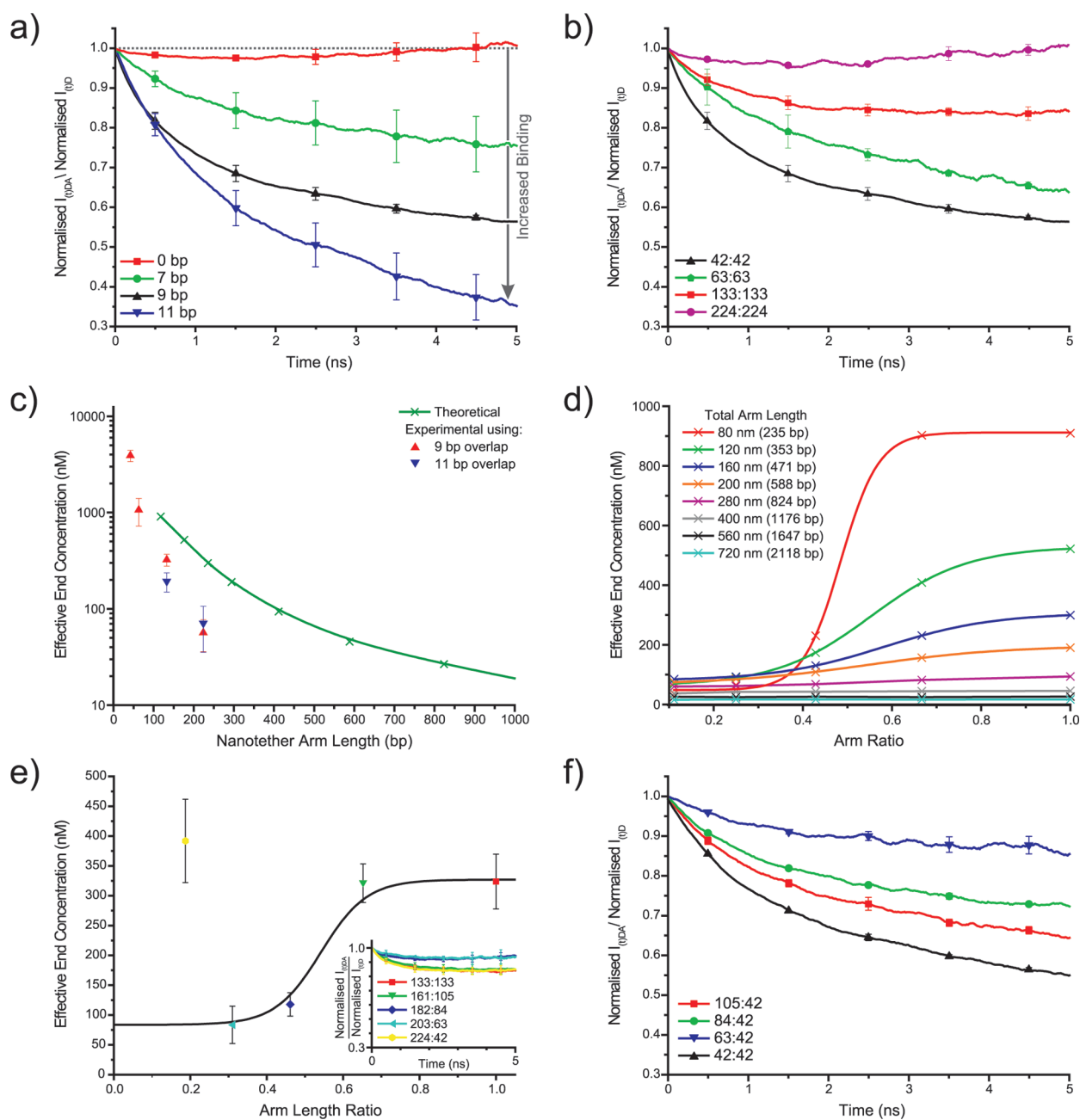


**Figure 3.** Tether length-dependent binding of surface associated nanotethers. (a) Higher affinity interactions (corresponding to longer length overlaps) show a greater fraction of bound donors as deduced from TR-FRET. The time-dependent donor fluorophore decay curve of headset pairs with or without an acceptor fluorophore was measured for the overlap lengths illustrated. The plateau ratio ( $I_{DA}/I_D$ ) directly relates to the proportion bound. (b) Tether length-dependent binding with a 9 bp overlap headset. Symmetrical tethers of the following length combinations showed distinct TR-FRET profiles (42:42, 63:63, 133:133, and 224:224). (c) Experimentally determined end concentrations compared favorably with those derived from Monte Carlo molecular simulations of nanotether dynamics. Experimental data shown as red and blue triangles for the 9 bp overlap and circles for the 11 bp overlaps, respectively; discrete numerical simulations are represented as crosses. (d) Simulation of a nanotether system with asymmetric arms of the same total length for each curve. Because of the stiffness of DNA close to its persistence length (150 bp), longer arms are less likely to bend and interact with shorter tethers than for equal length tethers of the same total length. (e) Effective end concentrations derived from the measured fraction of bound donors and the known affinity of 9 bp overlap in asymmetrical nanotether arms compared to the theoretical concentrations derived from simulations. The  $I_{DA}/I_D$  vs time plot for the various asymmetrical arms is shown in the insert. (f) Levels of binding observed with the 9 bp overlap headsets attached to asymmetrical nanotether arms of the differing total lengths (105:42, 84:42, 63:42) compared to that observed with the shortest synthesized symmetrical nanotether (42:42).

orientation of the single stranded breaks within the final tether structure. To further investigate the use of asymmetric arm lengths, a 42 bp arm was combined with a range of longer lengths

(Figure 3f). Of particular note from this analysis was the fact that the 63:42 ratio showed lower binding than the other asymmetrical arms tested. The lower effective concentration generated by

two of the shorter arm lengths may result from the stiffness of the 63 bp arm restricting its ability to bend back to interact with the 42 bp arm, while longer arms would have sufficient conformational flexibility to curve back and interact with the 42 bp arm. While the simulated and measured effective end concentrations generally followed the same trend, the experimentally derived values were generally lower than those from the simulations.

Combining both variable length tether arms (short total length) with asymmetric arm lengths produced a very effective means of controlling the effective end concentrations and therefore the proportion of bound biomolecules (Figure 3f). For example, the 64:42 nanotether configuration generated an effective end concentration of 240 nM (SD = 60 nM,  $n = 2$ ) while the nearest symmetrical tether, 42:42, gave an end concentration of 3.8  $\mu$ M (SD = 0.4  $\mu$ M,  $n = 5$ ). The concentrations generated by the variable-length tethers described here span a low affinity range that is highly relevant biologically but for which high masses of biomolecules are typically required in current quantitative affinity techniques (SPR, calorimetry). In the longer term, the careful control of tether and arm ratio together with the use of stiffer tether polymers (e.g., DX-DNA<sup>14,15</sup>) should allow the nanotether technique to probe a broader range of effective biological affinities.

## CONCLUSIONS

In this paper we have successfully demonstrated a mechanism for controlling biomolecule interactions through the use of variable length DNA tethers that generate effective end concentrations ranging from 56 nM to 3.8  $\mu$ M. Importantly, the number of biomolecules required for a single data point was as few as 0.1 fmol. This corresponds to 2.1 fmol for a seven point binding curve in triplicate and is several orders of magnitude lower than the number of molecules required for analysis of similar affinity biomolecules using SPR and calorimetry techniques.

In order to fully utilize the nanotether technology, the nanotether system needs to be used to measure protein–protein and protein–ligand interactions and this would require attachment of proteins, peptides, and small molecules to the DNA headsets. Initially proteins could be attached, via lysine or cysteine residues, to headset oligonucleotides containing thiol or amine linker groups using a bifunctional cross-linking reagent; such as 6-maleimidohexanoic acid *N*-hydroxysuccinimide ester (Figure S4 in the Supporting Information). Alternatively an intein mediated reaction between the protein and an cysteine-modified oligonucleotide could be used to generate the protein–oligonucleotide fusion.<sup>16</sup> Further developments might allow the exploitation of the low mass requirements by utilizing rapid small-scale protein production techniques (e.g., *in vitro* translation) that currently produce amounts of material that are too low for quantitative analysis.

## ASSOCIATED CONTENT

**S** Supporting Information. Additional information regarding the equipment used for the time-resolved FRET measurements, data analysis, oligonucleotide sequences, nanotether arm composition, optimization of the anchor surface density, headset titrations and a proposed method for measuring protein interactions using nanotethers. This material is available free of charge via the Internet at <http://pubs.acs.org>.

## AUTHOR INFORMATION

### Corresponding Author

\*E-mail: [daletc@cardiff.ac.uk](mailto:daletc@cardiff.ac.uk)

## ACKNOWLEDGMENT

The authors thank the Welsh Development Agency and the U.K. Technology Strategy Board for funding. The authors would also like to thank Dr. Stefan Lofas, Dr. Nick Thomas, and Prof. Lisa Hall for project management and discussion and Prof. Wolfgang Langbein and Sebastian Braun for advice on the TR-FRET experiments.

## REFERENCES

- (1) Schuck, P. *Annu. Rev. Biophys. Biomol. Struct.* **1997**, *26*, 541–566.
- (2) Bjelic, S.; Jelasarov, I. *J. Mol. Recognit.* **2008**, *21*, 289–311.
- (3) Singhal, A.; Haynes, C. A.; Hansen, C. L. *Anal. Chem.* **2010**, *82*, 8671–8679.
- (4) Uttamchandani, M.; Wang, J.; Yao, S. Q. *Mol. BioSyst.* **2006**, *2*, 58–68.
- (5) Miyawaki, A.; Llopis, J.; Heim, R.; McCaffery, J. M.; Adams, J. A.; Ikura, M.; Tsien, R. Y. *Nature* **1997**, *388*, 882–887.
- (6) Li, I. T.; Pham, E.; Truong, K. *Biotechnol. Lett.* **2006**, *28*, 1971–1982.
- (7) Tyagi, S.; Bratu, D. P.; Kramer, F. R. *Nat. Biotechnol.* **1998**, *16*, 49–53.
- (8) Shore, D.; Langowski, J.; Baldwin, R. *Proc. Natl. Acad. Sci. U.S.A.* **1981**, *78*, 4833–4837.
- (9) Rippe, K. *Trends Biochem. Sci.* **2001**, *26*, 733–740.
- (10) Hagerman, P. J. *Annu. Rev. Biophys. Biophys. Chem.* **1988**, *17*, 265–86.
- (11) Kasry, A.; Borri, P.; Davies, P. R.; Harwood, A.; Thomas, N.; Lofas, S.; Dale, T. *ACS Appl. Mater. Interfaces* **2009**, *1*, 1793–1798.
- (12) Klenin, K.; Merlitz, H.; Langowski, J. *Biophys. J.* **1998**, *74*, 780–788.
- (13) Levene, S. D.; Crothers, D. M. *J. Mol. Biol.* **1986**, *189*, 61–72.
- (14) Fu, T. J.; Seeman, N. C. *Biochemistry* **1993**, *32*, 3211–3220.
- (15) Winfree, E.; Liu, F.; Wenzler, L. A.; Seeman, N. C. *Nature* **1998**, *394*, 539–544.
- (16) Burbulis, I.; Yamaguchi, K.; Gordon, A.; Robert Carlson, R.; Brent, R. *Nat. Methods* **2005**, *2*, 31–37.